First-in-human demonstration of floating EMG sensors and stimulators wirelessly powered and operated by volume conduction

Laura Becerra-Fajardo[1], Jesus Minguillon[1,2,3], Marc Oliver Krob[4], Camila Rodrigues[5,6], Miguel González-Sánchez[7], Álvaro Megía-García[8], Carolina Redondo Galán[8], Francisco Gutiérrez Henares[8], Albert Comerma[1], Antonio J. del-Ama[9], Angel Gil-Agudo[8,10], Francisco Grandas[7], Andreas Schneider-Ickert[4], Filipe Oliveira Barroso[5,10], and Antoni Ivorra[1,11]*

Author details

[1]Department of Information and Communications Technologies, Universitat Pompeu Fabra, 08018 Barcelona, Spain.

[2]Research Centre for Information and Communications Technologies, University of Granada, 18014 Granada, Spain.

[3]Department of Signal Theory, Telematics and Communications, University of Granada, 18014 Granada, Spain.

[4]Fraunhofer Institute for Biomedical Engineering IBMT, 66280 Sulzbach, Germany.

[5]Neural Rehabilitation Group, Cajal Institute, Spanish National Research Council (CSIC), 28002 Madrid, Spain.

[6]Carlos III University of Madrid, Systems Engineering and Automation Department, 28903 Madrid, Spain.

[7]Movement Disorders Unit, Department of Neurology, Hospital General Universitario Gregorio Marañón, 28007 Madrid, Spain.

[8]Biomechanics and Assistive Technology Unit, National Hospital for Paraplegics. Unit of Neurorehabilitation, Biomechanics and Sensory-Motor Function (HNP-SESCAM), Unit associated to the CSIC, Toledo, Spain.

[9]School of Science and Technology, Department of Applied Mathematics, Materials Science and Engineering and Electronic Technology, Rey Juan Carlos University, 28933 Móstoles, Spain.

[10]CSIC's Associated RDI Unit 'Unidad De Neurorehabilitación, Biomecánica Y Función Sensitivo-Motora'

[11]Serra Húnter Fellow Programme, Universitat Pompeu Fabra, 08018 Barcelona, Spain.

*Correspondence: antoni.ivorra@upf.edu

Abstract

Background: Very recently we reported the design and evaluation of floating semi-implantable devices that receive power from and bidirectionally communicate with an external system using coupling by volume conduction.

The proposed approach, of which the semi-implantable devices are proof-of-concept prototypes, may overcome some of the limitations presented by existing neuroprostheses, especially those related to the size of the implantable devices and the need to perform complex surgical procedures. This is accomplished as the implants do not require rigid and bulky components within them and can be developed as flexible threadlike devices, a form factor that is beneficial for motor neuroprostheses. Here we report the first-in-human demonstration of these semi-implantable devices for both electromyography (EMG) sensing and electrical stimulation in an acute study.

Methods: A single floating device, consisting of implantable thin-film electrodes and a non-implantable miniature electronic circuit connected to them, was deployed in the upper or lower limb of six healthy participants. Two external textile electrodes were strapped around the limb and were connected to the external system, which delivered high frequency current bursts. Within these bursts, 13 different commands were modulated to communicate with the wireless implant. In one participant, isometric forces were measured while acquiring EMG activity of voluntary muscle contractions using the semi-implantable device.

Results: The floating EMG sensors and stimulators were successfully deployed in the biceps brachii and the gastrocnemius medialis muscles, and the external system was able to power them and bidirectionally communicate with them. Both sensing and stimulation parameters were configured externally using the communication protocol developed for the system. In one participant, both electrical stimulation and EMG acquisition assays were successfully performed, demonstrating the feasibility of the approach to power and communicate with the floating devices.

Conclusions: This is the first time that floating EMG sensors and electrical stimulators that are powered and communicate by volume conduction are demonstrated in humans. These devices, which can be highly miniaturized using current microelectronic technologies, open the possibility of using coupling by volume conduction in networked neuroprosthetics, obtaining fully implantable wireless devices with sensing and stimulation capabilities.

Keywords

wireless power transfer, volume conduction, AIMDs, bidirectional communications, electromyography, sensor, electrical stimulation, neuroprostheses, semi-implantable devices, human validation.

I. Background

Neuroprosthetic technologies based on active implantable medical devices (AIMDs) have the potential to be an important tool for improving the quality of life of patients with neurological disorders and patients that require external systems as prostheses and exoskeletons. For example, intramuscular microstimulators could be used to reduce pathological tremor in essential tremor patients, as intramuscular electrical stimulation has been shown to reduce tremor in this population of patients up to 24 h [1]. Moreover, intramuscular electromyography (EMG) microsensors could be used to control prostheses and exoskeletons [2][3][4], especially as it has been demonstrated to be a reliable input to feed neuromusculoskeletal models to estimate the user-intended joint movements for human-machine interface (HMI) control [5].

Implantable neuroprostheses form a chronic interface with the nervous system that overcomes one of the most important limitations of EMG sensors and electrical stimulators based on surface electrodes: the lack of selectivity. In addition, implantable electrodes improve repeatability by avoiding the impact of skin impedance changes and movements, and allow accessing deep muscles. In the case of EMG sensing for HMI, implantable electrodes avoid the need to replace the electrodes at each use (which in turn requires recalibration of the HMI) [6] and crosstalk, and allow the control of more degrees-of-freedom through the use of multiple electrodes [7].

Within the EXTEND collaborative project, funded by the European Commission and in which the authors of this study participate, it has been defined the concept of Bidirectional Hyper-Connected Neural Systems (BHNS). It refers to systems consisting of minimally invasive communication links between multiple nerves or muscles in the body and external devices which may be digitally interconnected between them (Fig. 1a). To achieve BHNS, we envision a dense network of wireless implantable devices that can act as stimulators and EMG sensors, and that communicate in real time with the external systems. The external systems, in turn, process and analyze the neuromuscular activity and control the stimulation and the action of machines (e.g., exoskeletons).

This BHNS paradigm requires fully implantable wireless devices that can be easily deployed by injection. Percutaneous systems would not be adequate to implement the BHNS concept because they require daily maintenance and dressing, and may present sweat gland blockage [7]. Most fully implantable devices are developed as a central pulse generator connected to electrodes through leads, which require complex surgical implantation procedures and tend to fail [8,9]. This approach would also not be adequate for the implementation of the BHNS

concept. To avoid the leads and their associated complications, it has been proposed the development of wireless networks of single-channel injectable devices that integrate the electrodes and the electronics. Nevertheless, the injectable devices capable of intramuscular stimulation that were developed in the past are stiff and relatively large (diameter > 2 mm) due to the need of batteries — with their limited lifespan and large volume [10], or to the need of components required for the wireless power transfer (WPT) method used to energize them (e.g., coils in inductive coupling [11–13]). Recently, WPT methods as inductive coupling, ultrasonic acoustic coupling and capacitive coupling have obtained high miniaturization levels at the expense of link efficiency, penetration depth, or functionality. Reviews on these methods can be found in [10,14–16].

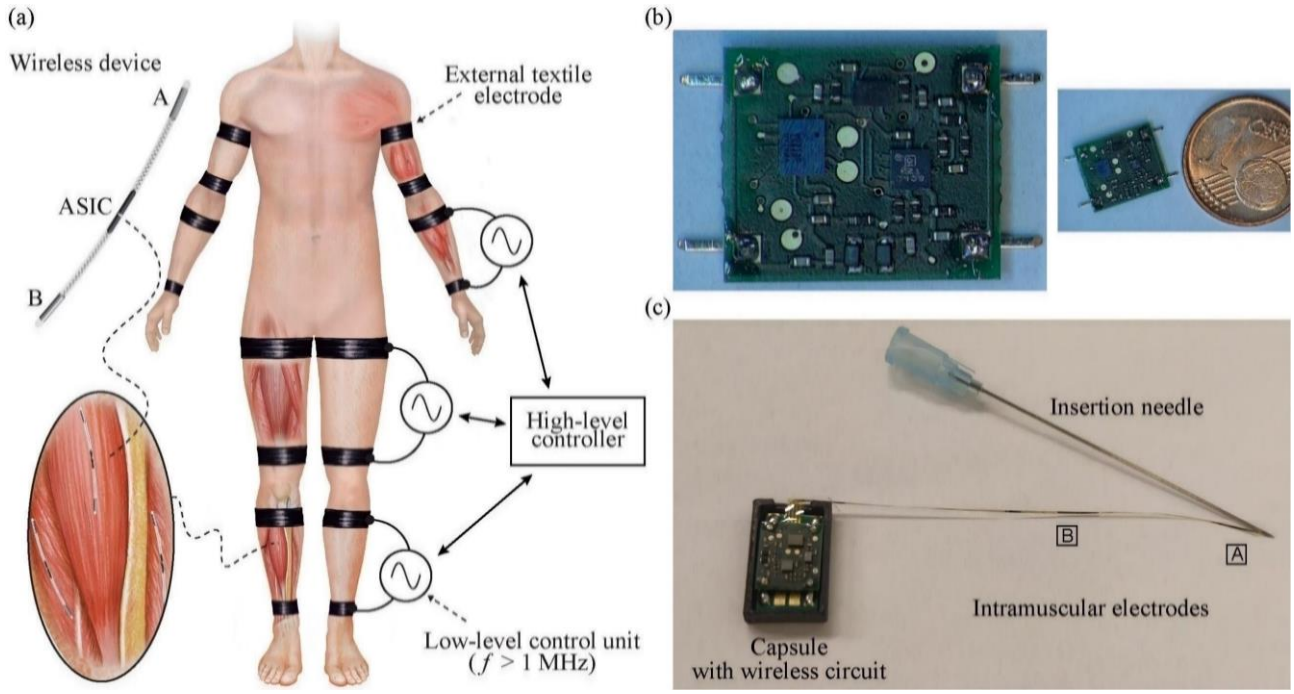

Fig. 1. Bidirectional Hyper-Connected Neural System (BHNS) concept and proof-of-concept semi-implantable devices. a) Schematic representation of the envisioned BHNS. b) Miniature electronic circuit for EMG sensing and stimulation and its comparison with a 1 cent euro coin for acute human demonstration of the BHNS concept. c) Complete semi-implantable device showing the dedicated insertion needle, the thin-film intramuscular electrodes, and the polymer capsule that houses the miniature circuit (opened lid) [17].

In the last years we have proposed and demonstrated a WPT method that avoids the use of bulky components inside the implant, and that allows to implement the implants as thin, flexible and elongated devices suitable for implantation by means of injection [18,19]. The implants are powered and controlled by applying — through textile electrodes — high frequency (HF) current bursts that flow through the tissues by volume conduction [20]. The currents are picked-up by the implant's electrodes (located at the ends of the elongated body, Fig. 1a) and are rectified for powering and bidirectional communications. This allows the integration of the electronics in an application-specific integrated circuit (ASIC). We have validated in humans that HF current bursts complying with

safety standards and applied through two textile electrodes strapped around a limb can provide substantial power from pairs of implanted electrodes, and are innocuous and imperceptible [21].

We have recently reported the development and evaluation of semi-implantable devices based on WPT by volume conduction that are capable both of performing stimulation and EMG sensing [17]. We also described the external system and a bidirectional communications protocol that allows wireless communication between the external system and the semi-implantable devices. The devices were evaluated using an agar phantom and in hindlimbs of anesthetized rabbits. Here we report the use of these semi-implantable devices in the limbs of healthy participants, a first-in-human demonstration of devices wirelessly powered and operated by volume conduction.

II. Methods

1. Electronic system

The electronic system consists of 1) an external system that delivers the HF current bursts for WPT and bidirectional communications, and 2) wireless devices for EMG sensing and electrical stimulation. This electronic system was extensively described in [17]. Yet some aspects are highlighted here to facilitate the reading of this first-in-human demonstration.

External system

The selected hierarchical architecture for the BHNS proposes the use of an external system that consists of one top-level controller that communicates with the wireless AIMDs through external low-level control units. These control units apply HF current bursts to the tissues to power and communicate with the wireless devices. The currents are applied using external textile electrodes strapped around the limbs (Fig. 1a).

The implemented control unit delivers HF bursts for powering. They include a single 30 ms “Power up” burst, and power maintenance bursts with a repetition frequency (F) of 50 Hz and duration (B) of 1.6 ms to keep energized the wireless implantable devices that are located between the external electrodes. To perform bidirectional communications, a custom communication protocol stack was created. In the case of downlink (i.e., information sent from the external system to the wireless devices), the bursts are amplitude modulated by the external system. A set of 13 different commands can be used to configure the sensing and stimulation parameters and control their execution. In the case of uplink (i.e., information sent from a wireless device to the external system), the external system delivers HF currents that are modulated, by means of load modulation, by the wireless devices to generate

an uplink reply that is seen by the external system as minute changes in current. The duration of the downlink and uplink bursts, as well as the EMG sensing and stimulation parameters that can be set from the external system are reported in [17].

Wireless devices for EMG sensing and electrical stimulation

As explained in [17], the wireless device for the acute human demonstration reported here consists of ultrathin intramuscular electrodes based on thin-film technology that are connected to a miniature electronic circuit to be fixed on the skin. Each device has only two double-sided electrodes on a narrow ribbon made of polyimide (coined Electrodes 'A' and 'B' in Fig. 1c) for powering, bidirectional communications, electrical stimulation, and EMG sensing. The distance between the electrodes' centers is 30 mm and the total surface area of each electrode is 3.8 mm^2. The miniature electronic circuit connected to the intramuscular electrodes (Fig. 1b) includes a microcontroller that has been programmed to run in three power consumption states to guarantee energy efficiency. The device is configured to power up and wait for instructions sent from the external system. For these human trials, the floating devices were double blister-packaged in clear Stericlin bags and heat sealed. The devices were sterilized by Ethylene oxide gas sterilization (8%) at low temperatures (38 - 42 °C).

2. Participants

The assays were performed at the Movement Disorders Clinic of Gregorio Marañón Hospital (Madrid, Spain) for the upper limb and at the Biomechanics and Assistive Technology Unit of National Hospital for Paraplegics (Toledo, Spain) for the lower limb. The procedures were conducted in accordance with the Declaration of Helsinki and approved by the local Ethics Committees (reference numbers 18/2020 and 565 respectively), as well as by the Spanish Agency of Medicines and Medical Devices (AEMPS) – records 858/20/EC and 856/20/EC respectively. Three healthy volunteers participated in the upper limb assays (23, 31, and 47 years old, all male), while other three healthy volunteers participated in the lower limb assays (29, 32 and 37 years old; two males, one female). The volunteers were recruited through a call for participation sent by email to colleagues and by another call posted in the facilities of both hospitals, and were not paid for their participation in the study. Before starting the experimental procedure, the participants were provided with oral and written information regarding the study (including risks, contingency measures, benefits, and data protection aspects) and signed an informed consent form.

3. Experimental Procedure

At first, the target muscle was defined for each participant. In the case of the upper limb, the target muscle was the biceps brachii or the triceps brachii; while in the lower limb it was the tibialis anterior, the gastrocnemius medialis or the gastrocnemius lateralis. A single semi-implantable floating EMG sensor and stimulator was set up per participant. Before inserting the thin-film electrodes of the semi-implantable device, the area was cleaned with chlorhexidine. The electrodes were implanted using the dedicated 23 G hypothermic needle (Sterican 4665600 by B. Braun Melsungen AG) having a length of 60 mm and an outer diameter of 0.6 mm (Fig. 1c). This procedure was guided by ultrasound to verify that the needle was correctly inserted in the muscle belly, and that its orientation was as parallel as possible to the skin (to maximize the alignment of the electrodes with the applied electric field delivered using the external textile electrodes). After the needle was inserted in the target location, the miniature electronic circuit (enclosed in a polymer capsule for protection) was fixed to the skin of the participant using adhesive tape to avoid the accidental extraction of the electrodes. Finally, the end of the guiding filament adhered to the Luer lock of the needle was cut, and the needle was gently extracted. Fig. 2 shows semi-implantable devices deployed in the biceps brachii of participant 2, and in the gastrocnemius medialis of participant 5.

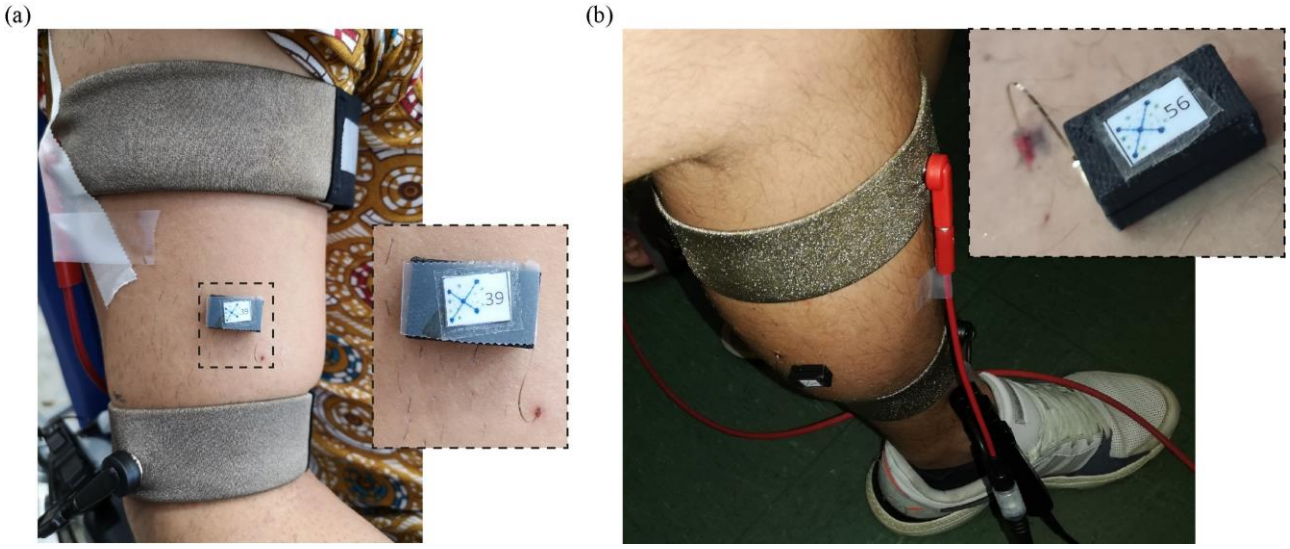

Fig. 2. Semi-implantable devices deployed in the target muscles of two participants. a) Device in biceps brachii of participant 2. b) Device in gastrocnemius medialis of participant 5.

Once the intramuscular electrodes were successfully inserted in the muscle belly, the textile electrodes were strapped around the limb and were connected to the external system. Several tests were performed to test the ability of the external system to power and bidirectionally communicate with the floating semi-implantable device. At first, “Pings” were requested from the external system. This implied that short communication frames that included a

device address were transmitted from the external system to the floating devices. If the address sent during downlink matched the address defined in the semi-implantable device, this device sent an acknowledge (ACK) frame to the external system. If this bidirectional communication trial was successful, longer communication frames were tested to guarantee that the external system could correctly configure the semi-implantable device for electrical stimulation and EMG sensing, trigger these functions (i.e., stimulate, start/stop sensing) and upload the samples of EMG activity acquired by the floating device.

After it was confirmed that the semi-implantable device was properly powered by the external system, and that the bidirectional communications were successful, electrical stimulation and EMG sensing assays were performed. In the case of electrical stimulation assays, videos were recorded to capture the moment in which a stimulation sequence was triggered from the external system. In the case of EMG sensing for biceps brachii assays, a force gauge was used to measure the tensile force exerted by the arm when the biceps brachii was contracted with the hand closed. The force gauge was attached firmly to the participant's arm – which was held in the armrest with an atraumatic band – and its base was fixed to a base of the chair, forcing an isometric contraction (Fig. 3). During this contraction, EMG was acquired by the floating device, and the samples were uploaded to the external system for offline analysis.

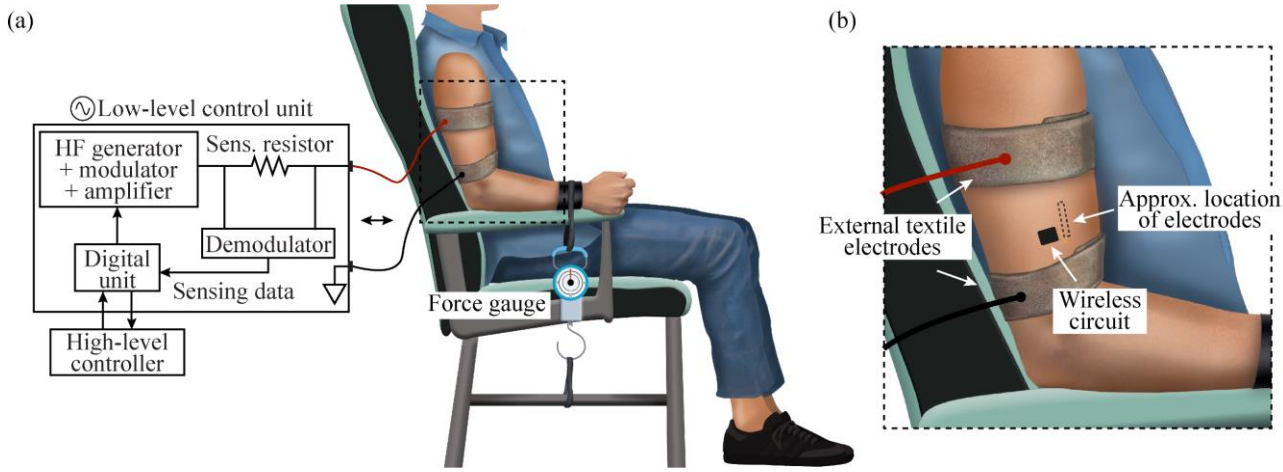

Fig. 3. Setup used during the study in upper limb. The participant was always sitting on a chair, and the external textile electrodes were connected to the external system. a) For the force measurement during isometric contractions of the biceps brachii, the wrist was strapped to the armrest of the chair, and to a force gauge. b) Zoom of the region where the wireless circuit was located, and approximate location of thin-film electrodes.

Each participant was constantly asked if he or she perceived any type of sensation related to the HF current bursts applied or to the floating device implanted, and the region close to the textile electrodes was visually monitored continuously. The surveillance also included measurements of the impedance across the external textile electrodes to identify possible changes in the interface between the textile electrodes and the skin. This was done

using an active differential probe (TA043 from Pico Technology Ltd) to measure the voltage applied across the external electrodes, and a current probe (TCP2020A from Tektronix, Inc.) to measure the HF current flowing through the tissues. Both probes were connected to a battery-powered oscilloscope (TPS2014 from Tektronix, Inc.).

After finalizing the assays, the external system was turned off and the textile electrodes were unstrapped. Then, the intramuscular electrodes were extracted by holding the guiding filament and the electrodes' filament and gently pulling out, and the insertion region on the skin was cleaned with chlorhexidine. The participants remained for 30 more minutes in the hospital for monitoring, and were monitored again 24 h later through a phone call to ensure their well-being and to note possible adverse effects.

III. Results

1. Implantation

The insertion mechanism was minimally invasive and did not require local anesthesia. In the case of the implantation procedure in the triceps brachii, due to limitations in the room, the position during implantation was uncomfortable for the physician. This hampered the correct insertion of the electrode, which broke during the implantation. In the case of the tibialis anterior and gastrocnemius lateralis muscles, the intramuscular electrodes broke during insertion as the dedicated needle experienced more stiffness due to the insertion angle required to maximize the alignment of the electrodes with the applied electric field. For these reasons, the study was finally performed in the biceps brachii and the gastrocnemius medialis.

Fig. 4 shows the ultrasound image obtained immediately after the needle was placed in the biceps brachii of participant 2. Only 3.4 cm of the 6 cm needle are seen in the image (limited by the ultrasound's transducer length), but the resulting insertion length was approximately 5.5 cm. The participant had a subcutaneous fat layer of approximately 3 mm, and the needle – corresponding to the position of the thin-film electrodes – had an angle of approximately 8º with respect to the skin. Table 1 summarizes the final location of the floating device in all the participants.

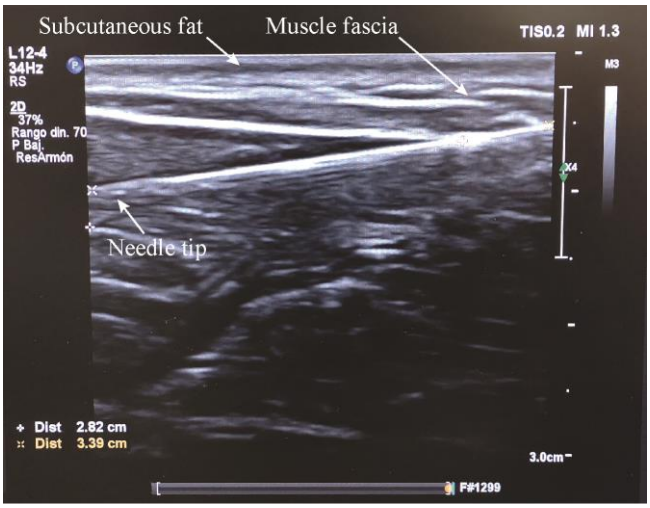

Fig. 4. Ultrasounds image obtained from participant 2 immediately after the needle was inserted in the biceps brachii. The needle was injected from the top right corner (not shown in the image), passed through subcutaneous fat and the muscle fascia, and ended up in the target muscle. The tip of the needle is seen at the left of the image at a depth of approximately 1 cm.

Table 1. Demographic information and bidirectional communications success rate in each participant

Participant	Gender	Age	Target muscle	Communications success rate
1	Male	47	Biceps brachii	No communication
2	Male	31	Biceps brachii	Ping: 100% Get Config: 100%
3	Male	23	Biceps brachii	Ping: 100%
4	Female	37	Gastrocnemius medialis	No communication
5	Male	29	Gastrocnemius medialis	Ping: 40%
6	Male	32	Gastrocnemius medialis	Ping: 80%

2. Bidirectional communications

Fig. 5 shows an example of the waveforms obtained from the external system when it requested a “Ping”, and the floating device replied with an ACK frame. The waveforms were obtained in the upper arm (Fig. 5a) and the lower leg (Fig. 5b and Fig. 5c) of three different participants. The external system was delivering HF bursts at a frequency of 1.1 MHz (power maintenance burst frequency *F*: 50 Hz, and duration *B*: 1.6 ms). For any uplink, the external system delivers a HF current burst to trigger the reply and give energy to the semi-implantable device (Fig. 5, blue waveform). The load modulation made by the floating device creates minute changes in the current flowing

through the external textile electrodes. This current is sensed by the external system's demodulator using a sensing resistor (Fig. 3). Fig. 5 — orange waveform — shows the output of the demodulation circuit after filtering and amplifying the voltage across this sensing resistor. This output latter passes by an analog comparator, whose output connects to the receiver of the external system's universal asynchronous receiver-transmitter (UART) to decode the information sent by the semi-implantable device. In the case of participant 2 (Fig. 5a), who had the semi-implantable device deployed in the biceps brachii, success rates of 100% were obtained for bidirectional communications, both in short frames as the "Ping" command, as well as in longer frames such as "Get Config" when the external system was delivering bursts with an amplitude of 60 V and 1.42 A, and the textile electrodes were separated 10 cm. For another upper limb participant, participant 3, success rates of 100% were obtained for pings to a device implanted in the biceps brachii. In the case of participant 5 (Fig. 5b), whose floating device was in the gastrocnemius medialis, the maximum success rate for pings was only 40% (68 V, 2.28 A, 10 cm distance between centers of textile electrodes). Its orange waveform clearly shows a HF component in the uplink waveform (i.e., output of demodulator of external system), which may have generated an incorrect digital signal in the comparator, therefore generating errors in the decoder. Additionally, the waveform shows low peak-to-peak variations during the ACK, which hampers even more the decoding of the data. In the case of participant 6 (Fig. **5**c), whose device was also implanted in the gastrocnemius medialis, the maximum success rate for pings was 80% (90 V, 2.1 A, 12 cm distance between textile electrodes). The orange uplink waveform also contains some HF component, but the ACK ping message differs clearly from the rest of the window.

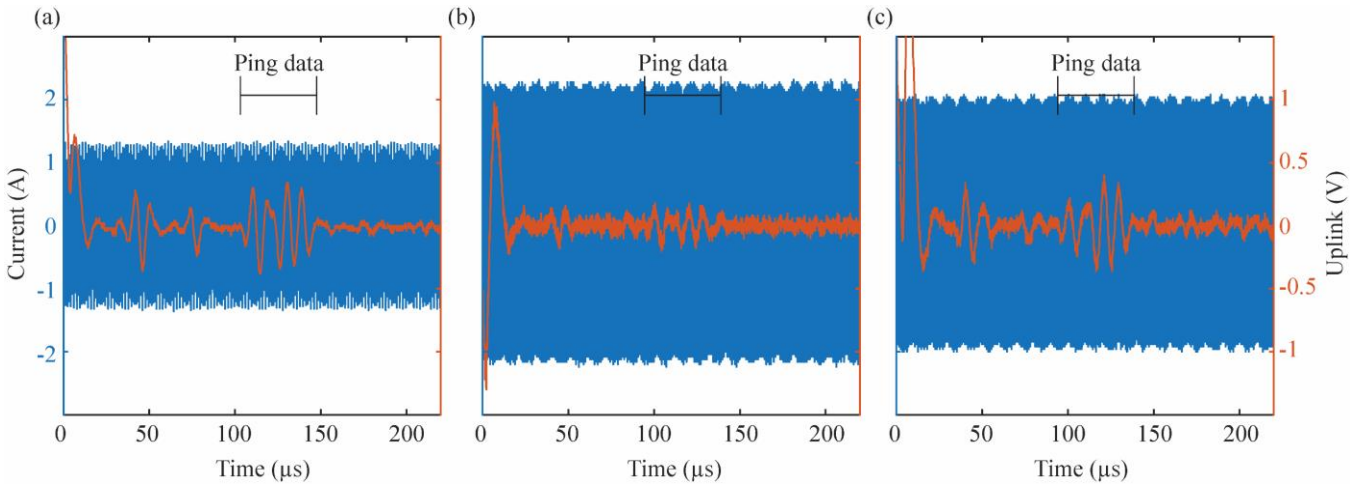

Fig. 5. Waveforms obtained with a floating oscilloscope and the probes connected to the external system. These waveforms are obtained after the external system requests a "Ping" to a specific device. In blue, HF current delivered by external system for uplink; in orange, output of external system's demodulator, showing the filtered and amplified voltage across the sensing resistor when the floating device does an ACK ping message by load modulating the HF current burst (i.e., shows changes in the current flowing through textile electrodes). a) Participant 2, biceps brachii. b) Participant 5, gastrocnemius medialis. c) Participant 6, gastrocnemius medialis.

The ping requests sent to the device implanted in the biceps brachii of participant 1 and the gastrocnemius medialis of participant 4 were not properly received by the external system. In both cases it is unclear whether the devices were not properly powered (e.g., because the proximal electrode ('B' in Fig. 1c) was lying in fat tissue), or whether the hardware-based demodulation and decoding circuit of the external system was not able to properly acquire and interpret the signal modulated by the floating devices when they were sending their ACK ping message (e.g., because the modulation index was too low for the digital converter to work properly).

3. Electrical stimulation and EMG sensing

As the semi-implantable device in participant 2 was able to be powered by and to bidirectionally communicate with the external system in both short and long communication frames, it was possible to configure the stimulation and EMG acquisition parameters of the floating device. To perform a stimulation sequence when the floating device was configured to do biphasic symmetric stimulation with a cathodic-first pulse (i.e., a cathodal phase is followed by an anodal phase to obtain a charge-balanced pulse [22]), the external system delivered HF current bursts to generate a stimulation with a frequency of 150 Hz, 120 µs pulse width and interphase dwell of 30 µs, with a maximum stimulation amplitude of 2 mA. The skin area over the region where the thin-film electrodes were located slightly sank – indicating muscle contraction – when the stimulation was triggered by the external system. Fig. 6 shows the initial position of the skin right before stimulation was triggered, and during stimulation.

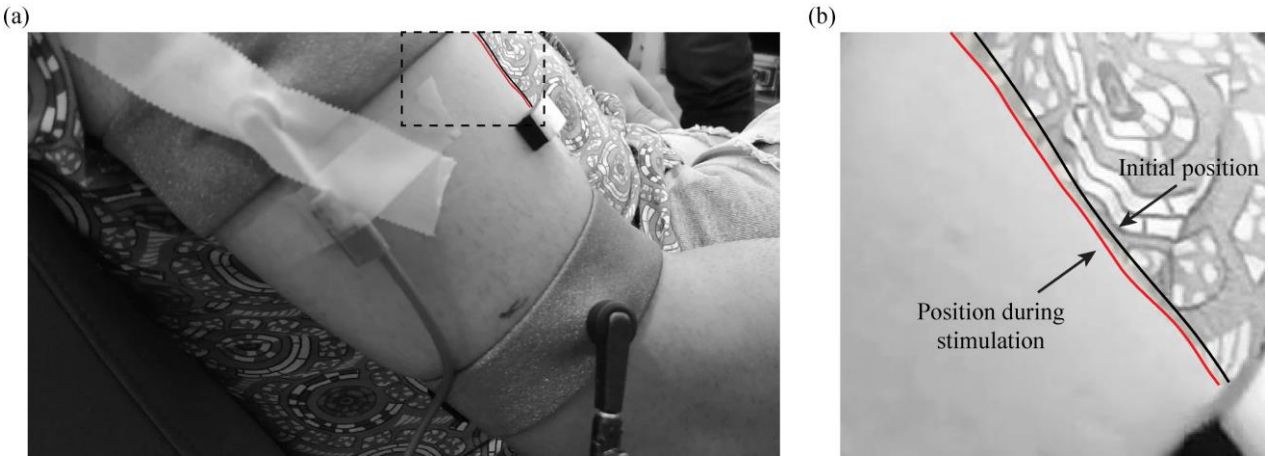

Fig. 6. Video frames during stimulation. a) Video frame showing the initial position of the skin over the biceps brachii few milliseconds before the semi-implantable device was triggered for stimulation. b) Zoom of the region marked in a) delineating the initial position of the muscle, and its position during stimulation.

In the case of EMG acquisition, it was possible to obtain raw EMG. Fig. 7a shows two raw waveforms recorded by the wireless device and transmitted to the external system: the baseline (blue) and a voluntary sustained

contraction done by the participant (orange). The floating device was configured to acquire raw EMG at a sampling rate of 1 ksps.

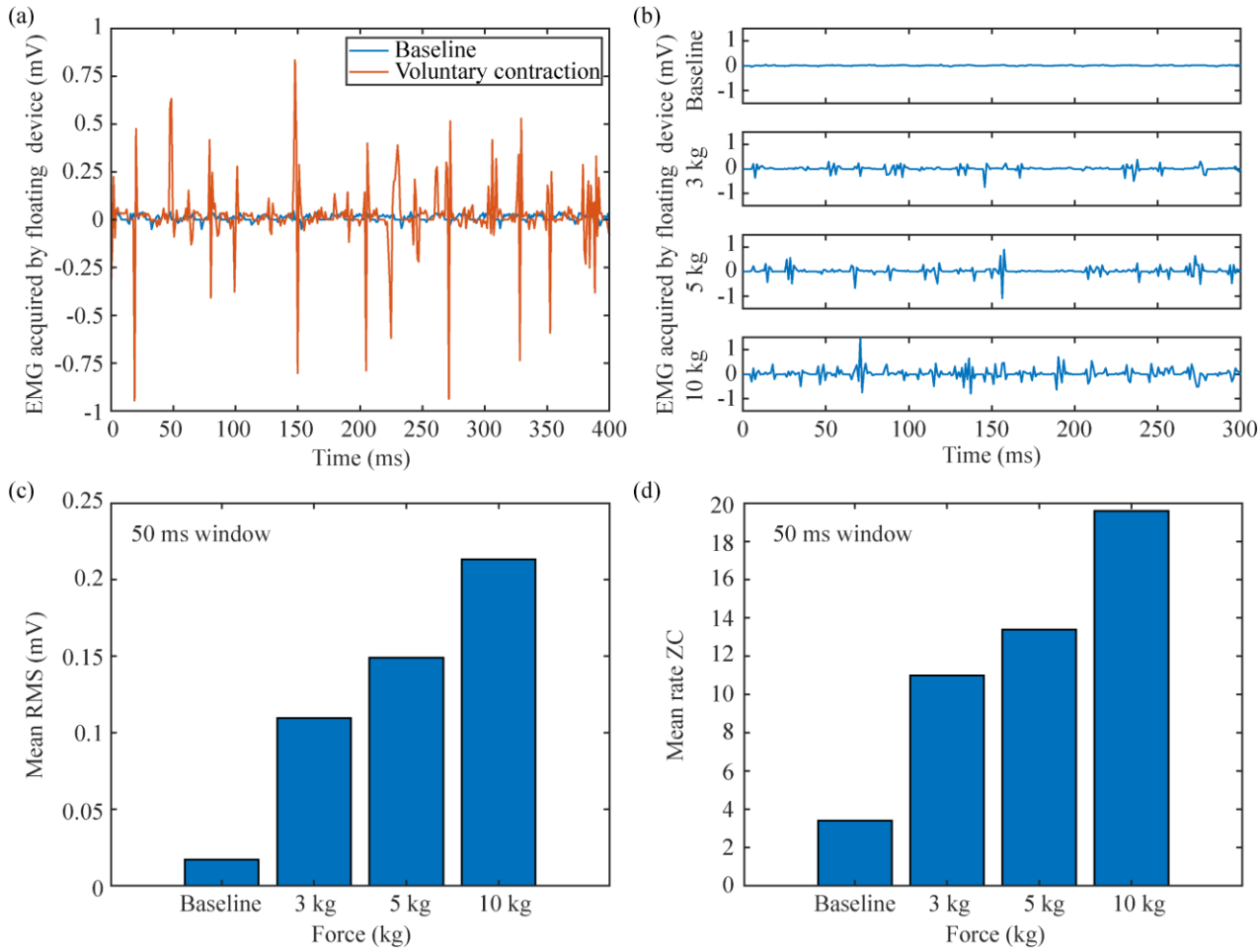

Fig. 7. Examples of raw EMG obtained by the floating EMG sensor and stimulator in biceps brachii of participant 2. A) Comparison between baseline and sustained contraction. b) Comparison between baseline and three different target forces exerted by the participant. c) Offline calculation of average of root mean square (RMS) value for the raw signals shown in b. d) Offline averaging of zero crossing (ZC) calculation for the raw signals shown in b. In both cases, the window used for calculation was set to 50 ms.

Using a force gauge as a reference (Fig. 3), participant 2 was asked to contract his arm to target a specific force. Fig. 7b shows raw EMG recordings obtained for four trials, corresponding to no contraction (baseline), 3 kg, 5 kg and 10 kg of force. As the target force increases, the electrical activity measured from the floating device increases. These raw signals were used to quantify offline the root mean square (RMS) value and the zero crossings (ZC) rate for specific time windows to evaluate its use in a future BHNS. RMS is an amplitude estimator while ZC, calculated by finding the rate of crosses by zero in the time domain, is an indicator of the changes of the spectral content of the EMG [23]. Fig. 7c-d show the mean RMS and mean ZC respectively for each raw signal, obtaining both parameters using a 50 ms window. As expected, both parameters increased when the force increased.

To avoid the limitations imposed by the internal memory of the miniature electronic circuit of the floating device, and to be more efficient with the communication channel by minimizing the amount of data to upload for the control of the BHNS, the floating device could internally calculate a parametric value of the obtained EMG. To limit the calculation time of the control unit (i.e., the amount of time it must be active in its higher power mode), it was considered that the parameters should be obtained from the signal in the time domain. One of these parameters is the rate of ZC, which is easier to implement in hardware [24]. A trial of parametric EMG based on ZC was done to evaluate the possibility of performing longer recordings. The floating device was configured to do EMG acquisition at a sampling rate of 1 ksps and parametrize the results using ZC with a window duration of 30 ms. The participant was asked to do three hard contractions in a 6 s frame (starting approximately at seconds 0, 2 and 4), while the semi-implantable device was acquiring the information. Fig. 8 shows the result of this assay, in which the three contractions can be clearly noticed. An offline moving average filter of 15 samples was used to highlight the envelope of the obtained parametric EMG.

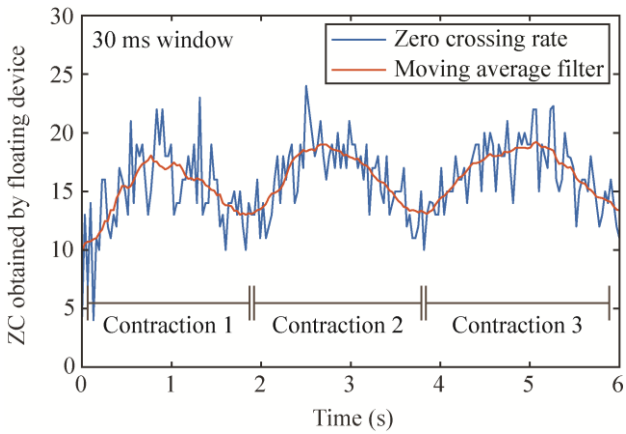

Fig. 8. Parametric acquisition using ZC rate. Participant 2 did three contractions during 6 seconds, which can be clearly seen by the parametric waveform obtained. After the samples were uploaded to the external system, a moving average filter was added to show the envelope of the contractions.

4. Extraction

After the assays were performed in the upper limb or lower limb of the participants, the intramuscular thin-film electrodes were gently extracted. The electrodes sled smoothly through the tissues, and both the main filament with the active sites of the electrodes and the thin guiding filament were extracted completely. There was no bleeding, pain, or secondary effects.

IV. Discussion

In this article, we have reported the first-in-human demonstration of floating devices powered and controlled by volume conduction, which are capable of EMG sensing and electrical stimulation. These semi-implantable devices were designed for the acute human study presented here and their technical implementation and *in vivo* validation were previously described [17].

Frequent breakage of the thin-film electrodes during their implantation was one of the most important limitations of the present study. In contrast to previous studies (upper limb [25][1], lower limb [26][27][28], neck [29][28], and hand [27][28] muscles) in which very similar thin-film electrodes were reproducibly implanted transversally to and/or shallower into the muscle, here the electrodes had to be deeply inserted longitudinally to the limb to guarantee 1) that both the distal and proximal electrodes ('A' and 'B' respectively in Fig. 1c) were inside muscle tissue, and 2) that the power picked up by the floating device during the assays was enough to power the miniature electronic circuit. To accomplish this, the needle had to be completely inserted as longitudinal as possible to the muscle, in acute angle with the skin and the muscle fascia. Remarkably, the muscle fascia is an anisotropic connective tissue [30–32] that has higher stiffness and strain in the longitudinal than the transverse direction [33]. This implies that the needle and the thin guiding filament faced higher mechanical resistance in this insertion scenario than in the typical scenario of use for this kind of thin-film electrodes (i.e., perpendicular to the muscle). In the case of the lower limbs the conditions are more detrimental, as the fascia (e.g., crural fascia in the lower leg) is thicker and stiffer because it helps stabilize the limb during locomotion [34], and lower limb muscles are stiffer than upper limb muscles, making it even more difficult to insert the dedicated needle. It is worth noting that the crural fascia in the anterior compartment (tibialis anterior muscle) is stiffer than in the posterior compartment (gastrocnemius medialis muscle) [35]. This would explain why it was more difficult to implant in the tibialis anterior than in the gastrocnemius muscles. It has been also experimentally determined that the stiffness of the gastrocnemius lateralis muscle is higher than that of gastrocnemius medialis muscle, explaining the reason why it was easier to implant the device in the gastrocnemius medialis muscle [36,37].

In here we report the use of a single floating device per participant. This limitation was mainly due to timing restrictions in the hospitals where the study was performed. We deemed sufficient to inject only one wireless device for EMG sensing and electrical stimulation to demonstrate the WPT and communication method based on volume

conduction. However, it must be noted that the designed communication protocol allows the control of up to 256 devices per low-level control unit, and the possibility to have several low-level units connected to a high-level controller. In fact, we have *in vitro* demonstrated that more than 10 floating devices can be wirelessly powered and digitally controlled from the external system [38].

In terms of the results obtained for bidirectional communications, it is worth noting that the demodulation performed by the external system consists in a rather simple hardware-based approach: the output of the analog amplitude demodulator is interfaced with the UART of the digital unit using an analog comparator. This approach has several limitations, including fixed thresholds and the impossibility to postprocess the digital data to recover lost bits. The limitations hinder the correct decoding of the control unit in certain scenarios. For example, as the electric potential across the thin-film electrodes decreases, the modulation index seen from the external system during uplink decreases too. This can be improved by replacing the current approach (i.e., analog comparator plus UART) by a more flexible approach based on digital processing: digital filters, comparators with adaptive thresholds and specific decoding algorithms. This could increase the success rate for uplink in unfavorable cases where low signal-to-noise ratio (SNR) is obtained.

The assays performed in the second participant were focused on transmitting raw EMG samples obtained by the floating device. It must be noted, however, that raw EMG acquisition would not allow real-time control, thus limiting the potential of the BHNS concept, as the floating device has limited memory capacity, and all the samples must be uploaded to the external system, occupying the entire physical channel during several milliseconds (approximately 1.35 ms per sample). By parametrizing the EMG signal in the floating devices it is possible to very substantially reduce the amount of bytes to be transmitted, thus allowing real-time control. We report an example using the rate of ZC, which is a basic parametric measurement obtained in the time domain. However, the communication protocol created allows us to use a second parametric measurement that can be implemented in the firmware of the floating devices (e.g., RMS, spike properties [39]). Using parametric measurements, it is possible to acquire much more samples, store them in the wireless device's memory, and be more efficient with the powering/communication channel to accomplish a BHNS system that can operate in real time to process and analyze the information obtained using the intramuscular electrodes, and activate the electrical stimulation or control external machines such as exoskeletons.

The floating device described in depth in [17] and demonstrated here in the upper and lower limb of healthy participants cannot be used for chronic studies, as the thin-film intramuscular electrodes may fail [40] and the skin access is prone to infections in the long term. However, the architecture of the miniature electronic circuit connected to these intramuscular electrodes can be integrated into an ASIC, as it is composed of typical electronic components that can be fabricated using current microelectronic technologies and manufacturing processes. This would allow to fully implant the wireless devices for chronic studies and future commercial use, obtaining flexible threadlike EMG sensors and stimulators that can be easily implanted by injection. Very recently we have demonstrated in the hindlimbs of two anesthetized rabbits that fully injectable microstimulators that include an ASIC housed in a hermetic capsule (overall diameter of 0.97 mm) are able to rectify these volume conducted HF bursts to cause local low frequency currents capable of stimulation [41].

V. Conclusions

This study reports the first-in-human demonstration of the use of coupling by volume conduction as a WPT and bidirectional communications method to operate networks of wireless EMG sensors and stimulators. The demonstrated floating devices, consisting of thin-film injectable intramuscular electrodes connected to a miniature electronic circuit, were powered by and communicated with an external system that delivered HF current in the form of bursts via two external textile electrodes strapped around the limb where the device was deployed. It was demonstrated that the external system can send digital commands to configure the EMG sensing and electrical stimulation parameters, to trigger the acquisition or the stimulation, and to upload samples. This first-in-human demonstration opens the possibility of using coupling by volume conduction in networked neuroprosthetic systems.

References

1. Pascual-Valdunciel A, Gonzalez-Sanchez M, Muceli S, Adan-Barrientos B, Escobar-Segura V, Perez-Sanchez JR, et al. Intramuscular stimulation of muscle afferents attains prolonged tremor reduction in essential tremor patients. IEEE Trans Biomed Eng. 2020;68(6):1768–76.
2. Salminger S, Sturma A, Hofer C, Evangelista M, Perrin M, Bergmeister KD, et al. Long-term implant of intramuscular sensors and nerve transfers for wireless control of robotic arms in above-elbow amputees. Sci Robot. 2019;4(32):eaaw6306.

3. Fleming A, Stafford N, Huang S, Hu X, Ferris DP, Huang HH. Myoelectric control of robotic lower limb prostheses: a review of electromyography interfaces, control paradigms, challenges and future directions. J Neural Eng. 2021;18(4):41004.

4. Koller JR, Jacobs DA, Ferris DP, Remy CD. Learning to walk with an adaptive gain proportional myoelectric controller for a robotic ankle exoskeleton. J Neuroeng Rehabil. 2015;12(1):1–14.

5. Jung MK, Muceli S, Rodrigues C, Megía-García Á, Pascual-Valdunciel A, del-Ama AJ, et al. Intramuscular EMG-Driven Musculoskeletal Modelling: Towards Implanted Muscle Interfacing in Spinal Cord Injury Patients. IEEE Trans Biomed Eng. 2022;69(1):63–74.

6. Young AJ, Hargrove LJ, Kuiken TA. The effects of electrode size and orientation on the sensitivity of myoelectric pattern recognition systems to electrode shift. IEEE Trans Biomed Eng. 2011;58(9):2537–44.

7. Dewald HA, Lukyanenko P, Lambrecht JM, Anderson JR, Tyler DJ, Kirsch RF, et al. Stable, three degree-of-freedom myoelectric prosthetic control via chronic bipolar intramuscular electrodes: a case study. J Neuroeng Rehabil. 2019;16(1):147.

8. Kilgore KL, Anderson KD, Peckham PH. Neuroprosthesis for individuals with spinal cord injury. Neurol Res. 2020 Jul 30;1–13.

9. Memberg WD, Polasek KH, Hart RL, Bryden AM, Kilgore KL, Nemunaitis GA, et al. Implanted neuroprosthesis for restoring arm and hand function in people with high level tetraplegia. Arch Phys Med Rehabil. 2014 Jun;95(6):1201-1211.e1.

10. Dinis H, Mendes PM. A comprehensive review of powering methods used in state-of-the-art miniaturized implantable electronic devices. Biosens Bioelectron. 2021;172:112781.

11. Kane MJ, Breen PP, Quondamatteo F, ÓLaighin G. BION microstimulators: A case study in the engineering of an electronic implantable medical device. Med Eng Phys. 2011;33(1):7–16.

12. Merrill DR, Lockhart J, Troyk PR, Weir RF, Hankin DL. Development of an implantable myoelectric sensor for advanced prosthesis control. Artif Organs. 2011 Mar;35(3):249–52.

13. Schulman JH. The Feasible FES System: Battery Powered BION Stimulator. Proc IEEE. 2008;96(7):1226–39.

14. Barbruni GL, Ros PM, Demarchi D, Carrara S, Ghezzi D. Miniaturised Wireless Power Transfer Systems for Neurostimulation: A Review. IEEE Trans Biomed Circuits Syst. 2020;14(6):1160–78.

15. Turner BL, Senevirathne S, Kilgour K, McArt D, Biggs M, Menegatti S, et al. Ultrasound-Powered Implants: A Critical Review of Piezoelectric Material Selection and Applications. Adv Healthc Mater. 2021;10(17):2100986.

16. Agarwal K, Jegadeesan R, Guo Y-X, Thakor N V. Wireless Power Transfer Strategies for Implantable Bioelectronics. IEEE Rev Biomed Eng [Internet]. 2017;10:136–61. Available from: http://ieeexplore.ieee.org/document/7879807/

17. Becerra-Fajardo L, Krob MO, Minguillon J, Rodrigues C, Welsch C, Tudela-Pi M, et al. Floating EMG Sensors and Stimulators Wirelessly Powered and Operated by Volume Conduction for Networked Neuroprosthetics. J Neuroeng Rehabil. 2022;19(57).

18. Ivorra A. Remote Electrical Stimulation by Means of Implanted Rectifiers. PLoS One. 2011;6(8):e23456.

19. Ivorra A, Becerra-Fajardo L, Castellví Q. In vivo demonstration of injectable microstimulators based on charge-balanced rectification of epidermically applied currents. J Neural Eng. 2015;12(6):66010.

20. Tudela-Pi M, Minguillon J, Becerra-Fajardo L, Ivorra A. Volume Conduction for Powering Deeply Implanted Networks of Wireless Injectable Medical Devices: A Numerical Parametric Analysis. IEEE Access. 2021;9:100594–605.

21. Minguillon J, Tudela-Pi M, Becerra-Fajardo L, Perera-Bel E, Ama AJ del-, Gil-Agudo A, et al. Powering Electronic Implants by High Frequency Volume Conduction: In Human Validation. IEEE Trans Biomed Eng. 2023;70(2):659–70.

22. Cogan SF. Neural Stimulation and Recording Electrodes. Annu Rev Biomed Eng. 2008;10(1):275–309.

23. Hägg G. Electromyographic fatigue analysis based on the number of zero crossings. Pflügers Arch [Internet]. 1981;391(1):78–80. Available from: https://doi.org/10.1007/BF00580699

24. Clancy EA, Negro F, Farina D. Single-channel techniques for information extraction from the surface EMG signal. Surf Electromyogr Physiol Eng Appl. 2016;91–125.

25. Muceli S, Poppendieck W, Hoffmann K-P, Dosen S, Benito-León J, Barroso FO, et al. A thin-film multichannel electrode for muscle recording and stimulation in neuroprosthetics applications. J Neural Eng. 2019 Apr 1;16(2):026035.

26. Muceli S, Poppendieck W, Holobar A, Gandevia S, Liebetanz D, Farina D. Accurate decoding of the spinal cord output in humans with implanted high-density electrode arrays. bioRxiv. 2022;

27. Negro F, Muceli S, Castronovo AM, Holobar A, Farina D. Multi-channel intramuscular and surface EMG decomposition by convolutive blind source separation. J Neural Eng. 2016;13(2):26027.

28. Muceli S, Poppendieck W, Negro F, Yoshida K, Hoffmann KP, Butler JE, et al. Accurate and representative decoding of the neural drive to muscles in humans with multi-channel intramuscular thin-film electrodes. J Physiol [Internet]. 2015 Sep 1;593(17):3789–804. Available from: http://doi.wiley.com/10.1113/JP270902

29. Luu BL, Muceli S, Saboisky JP, Farina D, Héroux ME, Bilston LE, et al. Motor unit territories in human genioglossus estimated with multichannel intramuscular electrodes. J Appl Physiol. 2018;124(3):664–71.

30. Pancheri FQ, Eng CM, Lieberman DE, Biewener AA, Dorfmann L. A constitutive description of the anisotropic response of the fascia lata. J Mech Behav Biomed Mater. 2014;30:306–23.

31. Sednieva Y, Viste A, Naaim A, Bruyère-Garnier K, Gras L-L. Strain assessment of deep fascia of the thigh during leg movement: an in situ study. Front Bioeng Biotechnol. 2020;8:750.

32. Stecco C, Pavan PG, Porzionato A, Macchi V, Lancerotto L, Carniel EL, et al. Mechanics of crural fascia: from anatomy to constitutive modelling. Surg Radiol Anat. 2009;31(7):523–9.

33. Eng CM, Pancheri FQ, Lieberman DE, Biewener AA, Dorfmann L. Directional differences in the biaxial material properties of fascia lata and the implications for fascia function. Ann Biomed Eng. 2014;42(6):1224–37.

34. Stahl VA. A biomechanical analysis of the role of the crural fascia in the cat hindlimb. Dissertation P, editor. Georgia Institute of Technology and Emory University; 2010.

35. Stecco C, Pavan P, Pachera P, De Caro R, Natali A. Investigation of the mechanical properties of the human crural fascia and their possible clinical implications. Surg Radiol Anat. 2014;36(1):25–32.

36. Huang J, Qin K, Tang C, Zhu Y, Klein CS, Zhang Z, et al. Assessment of passive stiffness of medial and lateral heads of gastrocnemius muscle, Achilles tendon, and plantar fascia at different ankle and knee positions using the MyotonPRO. Med Sci Monit Int Med J Exp Clin Res. 2018;24:7570.

37. Lall PS, Alsubiheen AM, Aldaihan MM, Lee H. Differences in Medial and Lateral Gastrocnemius Stiffness after Exercise-Induced Muscle Fatigue. Vol. 19, International Journal of Environmental Research and Public Health. 2022.

38. Becerra-Fajardo L, Minguillon J, Comerma A, Ivorra A. Networks of Injectable Microdevices Powered and Digitally Linked by Volume Conduction for Neuroprosthetics: a Proof-of-Concept. In: Under review. 2022.

39. Gabriel DA. Reliability of SEMG spike parameters during concentric. Electromyogr Clin Neurophysiol. 2000;40:423–30.

40. Oldroyd P, Malliaras GG. Achieving long-term stability of thin-film electrodes for neurostimulation. Acta Biomater. 2022;139:65–81.

41. García-Moreno A, Comerma-Montells A, Tudela-Pi M, Minguillon J, Becerra-Fajardo L, Ivorra A. Wireless networks of injectable microelectronic stimulators based on rectification of volume conducted high frequency currents. J Neural Eng. 2022;19(5):056015.

List of abbreviations

AIMDs: active implantable medical devices; EMG: electromyography; HMI: human-machine interface; BHNS: Bidirectional Hyper-Connected Neural Systems; WPT: wireless power transfer; HF: high frequency; ASIC: application-specific integrated circuit; AEMPS: Spanish Agency of Medicines and Medical Devices; ACK: acknowledge; UART: universal asynchronous receiver-transmitter; RMS: root mean square; ZC: zero crossings; SNR: signal to noise ratio.

Declarations

1. Ethics approval and consent to participate

The procedures were conducted in accordance with the Declaration of Helsinki and approved by the local Ethics Committees of the Movement Disorders Clinic of Gregorio Marañón Hospital – Madrid – and the Biomechanics and Assistive Technology Unit of National Hospital for Paraplegics – Toledo – (reference numbers 18/2020 and 565 respectively), as well as by the Spanish Agency of Medicines and Medical Devices (AEMPS) – records 858/20/EC and 856/20/EC respectively. The participants volunteered to participate in this study, were informed about the procedures and possible adverse effects, and signed the informed consent to participate.

2. Consent for publication

Not applicable

3. Availability of data and materials

The datasets used and/or analyzed during the current study are available from the corresponding author on reasonable request.

4. Competing interests

The authors declare that they have no competing interests.

5. Funding

This work has received funding from the European Union's Horizon 2020 research and innovation programme under grant agreement No. 779982 (Project EXTEND - Bidirectional Hyper-Connected Neural System). CR has been also partially funded by CSIC Interdisciplinary Thematic Platform (PTI+) NEURO-AGINGl+ (PTI-NEURO-AGING+). FOB thanks the financial support from the Spanish MCIN/AEI/10.13039/501100011033 and by the "European Union NextGenerationEU/PRTR" under Grant agreement IJC2020-044467-I. AI gratefully acknowledges the financial support by ICREA under the ICREA Academia programme.

6. Authors' contributions

LBF, JM, MGS, AMG, FOB and AI conceived and designed the study. LBF, JM, CR and AI developed the electronic hardware and the software. MOK, AS and AI designed and developed the intramuscular electrodes. LBF, JM, CR, MGS, AMG, CRG, FGH, FOB and AI conducted the experiment. LBF and JM performed data analysis and drafted the manuscript. MOK, CR, MGS, AMG, CRG, FGH, AC, AJA, AGA, FG, AS, FOB and AI revised the manuscript critically. All authors read and approved the final manuscript.

7. Acknowledgements

The authors would like to express their gratitude to the participants of this study, and to Alejandro Pascual-Valdunciel and Juan Camilo Moreno for their support regarding the documentation for ethical committees and the AEMPS.